Impact of the Atlantic meridional overturning circulation on ocean heat storage and transient climate change

Yavor Kostov[1], Kyle C. Armour[1], and John Marshall[1]

[1] Department of Earth, Atmospheric, and Planetary Sciences, Massachusetts Institute of Technology, Cambridge, Massachusetts, USA

Abstract We propose here that the Atlantic meridional overturning circulation (AMOC) plays an important role in setting the effective heat capacity of the World Ocean and thus impacts the pace of transient climate change. The depth and strength of AMOC are shown to be strongly correlated with the depth of heat storage across a suite of state-of-the-art general circulation models (GCMs). In those models with a deeper and stronger AMOC, a smaller portion of the heat anomaly remains in the ocean mixed layer, and consequently, the surface temperature response is delayed. Representations of AMOC differ vastly across the GCMs, providing a major source of intermodel spread in the sea surface temperature (SST) response. A two-layer model fit to the GCMs is used to demonstrate that the intermodel spread in SSTs due to variations in the ocean's effective heat capacity is significant but smaller than the spread due to climate feedbacks.

1. Introduction

Forced with greenhouse gases (GHGs), the climate system adjusts toward a new equilibrium on various time scales: ultrafast responses in the stratosphere and troposphere (days and weeks), fast responses of the land surface and the ocean's mixed layer (months and years), and a long-term adjustment of the deeper ocean (decades to millennia) [e.g., *Gregory*, 2000; *Stouffer*, 2004; *Gregory and Webb*, 2008; *Held et al.*, 2010; *Andrews et al.*, 2012]. The ocean response time scales depend not only on the rate at which energy is absorbed at the sea surface (the net ocean heat uptake) but also on the efficiency with which that energy is transported away from the surface and into the ocean interior [e.g., *Hansen et al.*, 1985]. While early ocean models represented the downward propagation of the warming signal as a diffusive [e.g., *Hansen et al.*, 1985] or an upwelling-diffusive process [e.g., *Hoffert et al.*, 1980; *Wigley and Raper*, 1987; *Raper and Cubasch*, 1996], modern general circulation models (GCMs) reveal a variety of important vertical heat transport processes at work, such as stirring along sloped isopycnals and advection by the mean ocean circulation [e.g., *Gregory*, 2000]. Moreover, analyses suggest that differences in ocean heat uptake may play an important role for the large intermodel spread in simulated warming [*Raper et al.*, 2002; *Boé et al.*, 2009; *Hansen et al.*, 2011; *Kuhlbrodt and Gregory*, 2012; *Geoffroy et al.*, 2013a, 2013b]. Thus, key questions are as follows: what physical processes regulate the depth of ocean heat storage, and to what extent do they influence the surface climate response to GHG forcing?

We investigate these questions within the suite of state-of-the-art GCMs participating in the Coupled Model Intercomparison Project phase 5 (CMIP5) [*Taylor et al.*, 2012]. In particular, we analyze standardized simulations in which the atmospheric concentration of CO_2 is instantaneously quadrupled ($4 \times CO_2$) from its initial preindustrial value and then held fixed, providing a source of constant forcing for the climate system. In response to this idealized GHG perturbation, heat is taken up by the World Ocean. Part of the excess thermal energy remains in the topmost (~100 m deep) mixed layer of the ocean, and sea surface temperatures (SSTs) rise (Figure 1a). A substantial amount of heat also penetrates well below the mixed layer, but the vertical distribution of warming differs considerably across models (Figure 1b).

Here we propose that the upper cell of the Atlantic meridional overturning circulation (AMOC) is central to transporting and redistributing thermal energy to depth, thus regulating the effective heat capacity of the ocean under global warming. Moreover, we show that CMIP5 models differ substantially in their representation of the strength and depth of the AMOC and that this diversity largely accounts for the variability in the vertical distribution of ocean heat storage shown in Figure 1b.
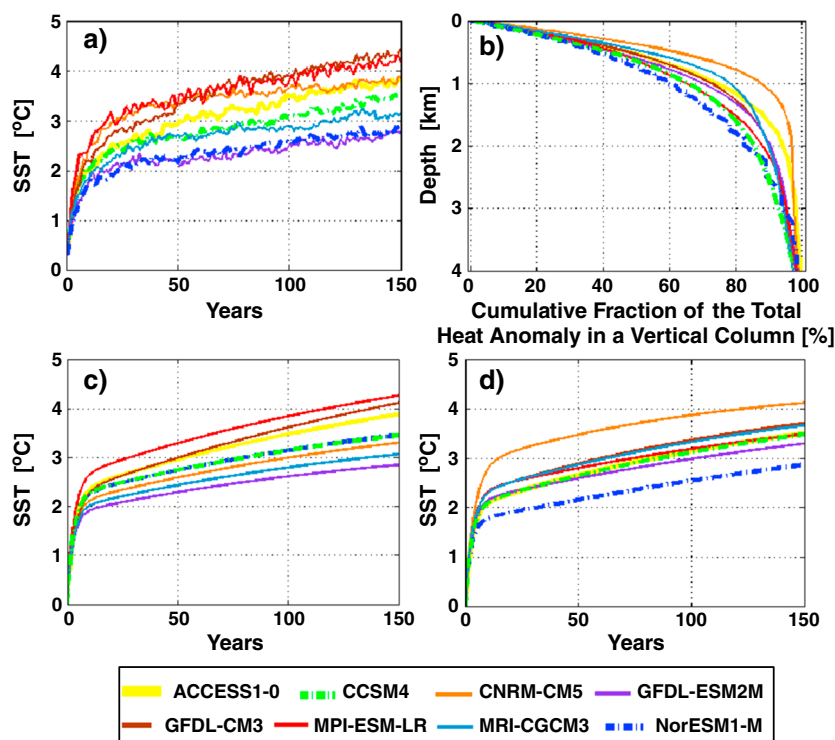
Figure 1. (a) Area-averaged SST anomaly in CMIP5 $4 \times CO_2$ simulations ; (b) Vertical distribution of the ocean heat anomaly in CMIP5 models, averaged over the World Ocean, 100 years after the CO_2 quadrupling; (c) SST response under model-specific feedback and forcing (λ_o, $\mathcal{F}_o$), but ensemble-mean ocean properties (q, h_2, ε), as simulated by the two-layer ocean energy balance model (EBM) (see section 3); (d) SST response under model-specific ocean properties (q, h_2, ε) but ensemble-mean feedback and forcing (λ_o, $\mathcal{F}_o$), as simulated by the two-layer ocean EBM (see section 3). The eight CMIP5 models included here are those for which sufficient output was accessible at the time of our analysis (ocean temperature, sea surface heat flux, and AMOC data).

To assess the influence of the effective ocean heat capacity on the surface climate response to forcing, we introduce a two-layer energy balance model, similar in form to that developed in *Gregory* [2000] and *Held et al.* [2010]. Such models have successfully reproduced the global temperature response in a wide range of GCMs [e.g., *Gregory*, 2000; *Held et al.*, 2010; *Li et al.*, 2012; *Geoffroy et al.*, 2012, 2013a, 2013b]. We similarly fit our two-layer model to global SSTs from $4 \times CO_2$ simulations, but we extend our analysis to interpret the model parameters in terms of physical processes. In particular, we find that the calibrated ocean heat capacity and rate of heat sequestration into the ocean interior are strongly correlated with the depth of heat penetration within the coupled GCMs, which, in turn, appears to be regulated by the vertical extent and strength of the AMOC cell. Finally, we use the two-layer ocean model to quantify the relative contributions of effective ocean heat capacity and climate feedbacks to the intermodel spread in SST response to forcing.

2. AMOC and Ocean Heat Storage

In order to evaluate the ocean's role in transient climate change, we analyze the relationship between warming at the sea surface and the distribution of stored heat with depth (see Figure S1 in the supporting information for the relationship between warming over land and ocean domains). We compute the area-averaged SST ($\equiv T_1$) and sea surface heat flux ($\equiv N_o$) anomalies over the global ocean by subtracting the linear trend of the preindustrial control from each corresponding $4 \times CO_2$ simulation. This eliminates unforced drift without adding noise [*Andrews et al.*, 2012]. Figure 1a shows the notable spread in transient SST responses across the ensemble of GCMs.

The rate of net ocean heat uptake N_o is defined as positive into the ocean and includes net shortwave and longwave radiation, as well as latent and sensible heat fluxes at the air-sea interface. Following CO_2 quadrupling, N_o is initially on the order of 10 W m^{-2} (Table S1) and decreases as the climate evolves toward a new equilibrium. The heat anomaly is initially concentrated in the ocean mixed layer but, over time, penetrates to
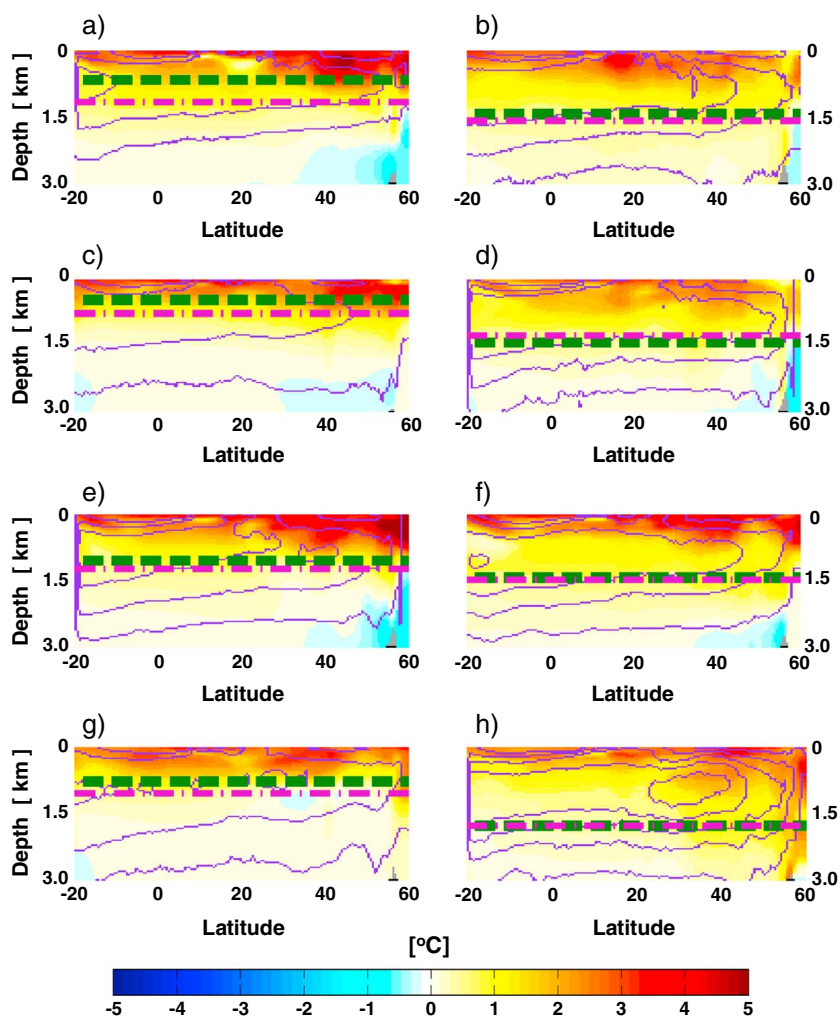
Figure 2. Zonal mean potential temperature anomaly in the World Ocean; 30 year average centered 100 years after $4\times CO_2$. The magenta dash-dotted line marks the average depth above which 80% of the heat anomaly is contained. Overlayed contours mark the upper overturning cell of the AMOC (Sv) between 35°S and the Arctic Circle (temporal average over the 150 year $4\times CO_2$ simulation; contour lines are 5 Sv apart, with an outermost contour at 0 Sv). The green dashed line denotes the uniform metric for the downward extent, D_{AMOC}, of the upper overturning cell. CMIP5 models: (a) ACCESS1-0, (b) CCSM4, (c) CNRM-CM5, (d) GFDL-ESM2M, (e) GFDL-CM3, (f) MPI-ESM-LR, (g) MRI-CGCM3, and (h) NorESM1-M.

ever increasing depth. A century after CO_2 quadrupling, warming can be seen at depths of several kilometers (Figure 2), but there exists a substantial intermodel spread. Indeed, Figure 1b shows that a large fraction of global ocean warming occurs below 1 km in some models (e.g., about 40% for NorESM1-M), while relatively little warming occurs below this depth in others (e.g., about 10% for CNRM-CM5). We define a metric for heat penetration, $D_{80\%}$, as the depth above which 80% of the total global heat content anomaly is contained after one century. $D_{80\%}$ varies considerably across models (Figure 2, horizontal magenta lines), with NorESM1-M ($D_{80\%} = 1.8$ km) and CNRM-CM5 ($D_{80\%} = 0.8$ km) as end members.

Various heat transport processes contribute to the distribution of heat storage with depth [e.g., *Gregory*, 2000]. Here we propose that the intermodel spread can be largely understood in terms of the different representations of AMOC among the GCMs. The overturning circulation affects vertical heat storage via two main mechanisms: ventilation of the ocean to depth of several km; and redistribution of the background heat content as the AMOC itself changes in response to surface wind and buoyancy forcing [e.g., *Xie and Vallis*, 2011; *Winton et al.*, 2013; *Rugenstein et al.*, 2013] (see supporting information).

To assess the overall impact of the AMOC, we consider its temporal average over the course of the $4 \times CO_2$ simulations. The volume overturning stream functions in the Atlantic-Arctic Basin of each model are shown
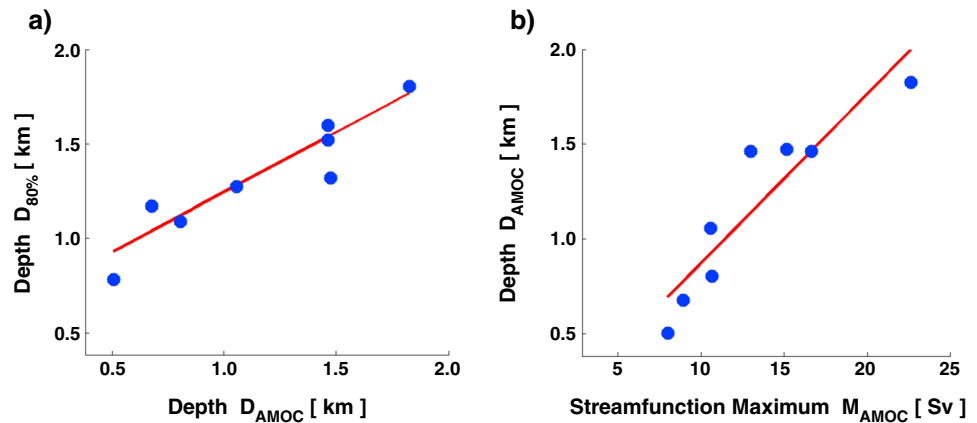
Figure 3. (a) Correlation between $D_{80\%}$ and D_{AMOC} ($R = 0.93$, p value $p < 0.01$); (b) Correlation between D_{AMOC} and M_{AMOC} ($R = 0.92$, p value $p < 0.01$).

in Figure 2. We define a metric for the vertical extent of the upper AMOC cell ($\equiv D_{AMOC}$) as the average depth of the 5 and 10 Sv streamlines in the Atlantic Ocean north of the 35°S parallel (Figure 2, horizontal green lines). D_{AMOC} varies from 0.5 km (CNRM-CM5) to 1.8 km (NorESM1-M) and is highly correlated (R=0.93) with the depth of heat penetration $D_{80\%}$ across the models (Figures 2 and 3a). D_{AMOC} also scales with the maximum of the stream function ($\equiv M_{AMOC}$; see Figure 3b). This result suggests that the propagation of the heat anomaly at depth may be linked both to the vertical extent and to the rate of overturning of the upper AMOC cell. The correlation between D_{AMOC} and M_{AMOC} themselves implies that stronger cells also tend to ventilate greater depths, but we acknowledge that this relationship may be intrinsic to our definition of D_{AMOC}. Note that these results are robust with respect to different definitions of D_{AMOC} and $D_{80\%}$ (see supporting information).

The important role of AMOC in setting the depth of ocean heat storage becomes clear when we consider the model-mean pattern of the net surface heat flux anomaly (Figure 4a). Surface heat uptake between 35°N and 70°N in the North Atlantic accounts for almost half of the net uptake by the World Ocean. Moreover, the horizontal pattern of anomalous heat distribution at intermediate depths suggests advection of heat along the AMOC cell. We see that the temperature anomaly at a depth of 1 km is particularly large along the Western Boundary of the Atlantic Ocean and appears to propagate from north to south over time along the lower limb of the upper AMOC cell (Figures 4b and 4c). In contrast, the Pacific and Indian Oceans do not show large heat anomalies at the same depth.

These results suggest that the AMOC plays a large role in setting the vertical distribution of the global ocean heat anomaly. We next assess the extent to which AMOC accounts for intermodel variability in the ocean's effective heat capacity as diagnosed from the transient SST response to forcing.

## 3. Ocean Heat Storage and SST Response

We fit an idealized two-layer ocean energy balance model (EBM) to the SST and the sea surface heat flux anomalies from each CMIP5 GCM. The two layers in the EBM broadly represent the mixed layer and deeper ocean, with respective temperature anomalies T_1 and T_2. Similar two-layer models have been studied extensively and shown to successfully capture the response of coupled GCMs [e.g., *Gregory*, 2000; *Held et al.*, 2010; *Geoffroy et al.*, 2012, 2013a, 2013b]. However, unlike previous applications of this EBM, we attempt to understand the idealized model in terms of key oceanic processes and mechanisms that affect the transient climate response. We thus treat land and the atmosphere as external to our system and formulate the model as follows.

The temperature anomalies in the two ocean layers, T_1 and T_2, evolve according to

$$c_w \rho_0 h_1 \frac{dT_1}{dt} = \mathcal{F}_o - \lambda_o T_1 - \varepsilon q (T_1 - T_2), \tag{1}$$

$$c_w \rho_0 h_2 \frac{dT_2}{dt} = q (T_1 - T_2), \tag{2}$$
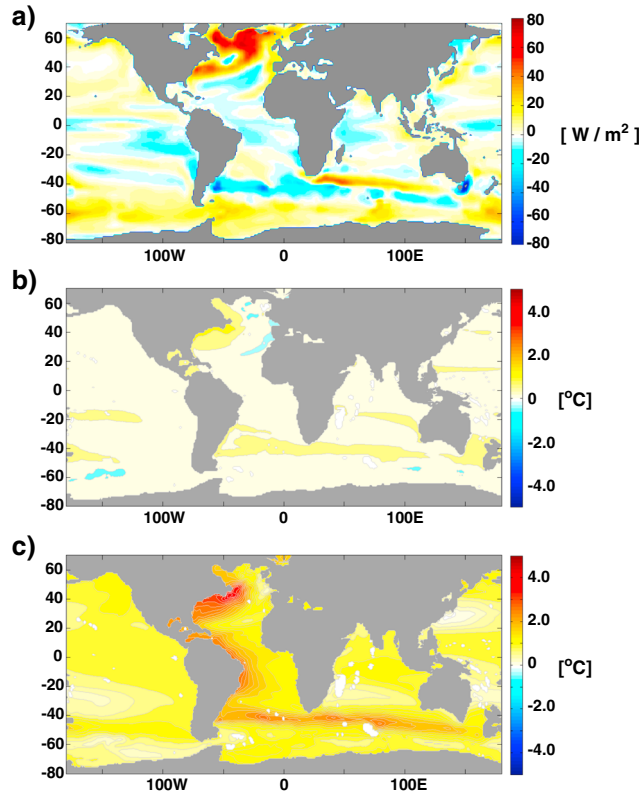
Figure 4. (a) CMIP5 $4 \times CO_2$ ensemble mean of (a) net heat flux anomaly at the ocean surface (30 year average centered on year 100); (b) potential temperature anomaly at depth 1000 m (30 year average centered on year 15); (c) potential temperature anomaly at depth 1000 m (30 year average centered on year 100).

where c_w and ρ_0 are the specific heat and the reference density of sea water, respectively; h_1 and h_2 are the thicknesses of the two ocean layers; λ_o (units: W m^{-2} K^{-1}) is a climate feedback parameter relating the surface heat flux to the SST; and the term $q(T_1 - T_2)$ (units: W m^{-2}) represents the rate of heat exchange between the mixed layer and deep ocean; parameter ε is discussed below. When atmospheric CO_2 is abruptly quadrupled, the upper ocean layer is forced with an energy flux $\mathcal{F}_o(t)$ approximated as a step function (units: W m^{-2}). $\mathcal{F}_o$ includes a contribution from heat exchange between the land and the ocean domain and therefore should be interpreted as an effective forcing on the ocean surface (see supporting information).

Within the GCMs the pattern of sea surface heat uptake is not geographically uniform (e.g., Figure 4a) and evolves in time as the ocean warms. Moreover, the climate feedbacks, which set the SST damping rate, are sensitive to the pattern of ocean heat uptake, and thus a different set of feedbacks are in operation at various stages of the climate response to forcing [*Winton et al.*, 2010; *Armour et al.*, 2013; *Rose et al.*, 2014]. To account for this effect within our idealized, global ocean model, we include a nondimensional "efficacy" factor $\varepsilon \sim \mathcal{O}(1)$ in equation (1), following *Held et al.* [2010]. A time-invariant ε is able to capture much of the nonlinear relationship between the surface heat flux and the SST found in the GCMs (see supporting information). Hence, we interpret λ_o as a time-invariant feedback that represents the relationship between equilibrium warming and forcing: $T_{eq} = \mathcal{F}_o/\lambda_o$.

The net sea surface heat flux N_o is equal to the total heat content change in the two ocean layers (the sum of equations (1) and (2)):

$$N_o = \mathcal{F}_o - \lambda_o T_1 - (\varepsilon - 1)q(T_1 - T_2) \qquad (3)$$

This budget provides a constraint for calibrating the idealized two-layer system to the GCMs. For simplicity, we prescribe a mixed layer depth of $h_1 = 100$ m. We thus have five free model parameters to fit: $\mathcal{F}_o, \lambda_o, \varepsilon, q,$ and h_2. Finally, the total EBM depth scale is the sum of the two layer thicknesses: $H = h_1 + h_2$.

We then define the rescaled variables $q' = \varepsilon q$ and $h'_2 = \varepsilon h_2$ to simplify equations (1) and (2) as follows:

$$c_w \rho_0 h_1 \frac{dT_1}{dt} = \mathcal{F}_o - \lambda_o T_1 - q'(T_1 - T_2) \qquad (4)$$

$$c_w \rho_0 h'_2 \frac{dT_2}{dt} = q'(T_1 - T_2). \qquad (5)$$

This new system of equations has an analytical solution for the evolution of the SST anomaly T_1 in response to step forcing:

$$T_1(t) = T_{eq} - T_F e^{-\sigma_1 t} - (T_{eq} - T_F)e^{-\sigma_2 t}. \qquad (6)$$

The SST anomaly approaches the equilibrium value $T_{eq} = \mathcal{F}_o/\lambda_o$ on two exponential time scales: a fast ($1/\sigma_1$) and a slow ($1/\sigma_2$) time scale of response [*Held et al.*, 2010]. We can expand the rates σ_1 and σ_2 in terms of a nondimensional ratio of layer thicknesses, $r = h_1/h_2' = h_1/(\varepsilon h_2) \ll 1$ to express

$$\sigma_1 = \frac{\lambda_o}{c_1}\left[1 + \frac{q'}{\lambda_o} + \frac{q'^2}{\lambda_o(\lambda_o + q')}r + \mathcal{O}(r^2)\right]$$
$$\approx \frac{\lambda_o + q'}{c_1} \tag{7}$$

$$\sigma_2 = \frac{\lambda_o}{c_1}\left[\frac{q'}{(\lambda_o + q')}r + \mathcal{O}(r^2)\right] \approx \frac{1}{c_1}\left(\frac{\lambda_o q' r}{\lambda_o + q'}\right), \tag{8}$$

where $c_1 = c_w \rho_0 h_1$ is the constant heat capacity of the upper ocean layer. The fast SST response T_F is the fraction of the temperature anomaly that the ocean surface reaches on a time scale $1/\sigma_1$ and can be expressed as

$$T_F = \frac{\mathcal{F}_o}{\lambda_o}\left[\frac{\lambda_o}{\lambda_o + q'} - \frac{2\lambda_o q'^2}{(q' + \lambda_o)^3}r + \mathcal{O}(r^2)\right] \approx \frac{\mathcal{F}_o}{\lambda_o + q'}. \tag{9}$$

Beyond the fast response, the equilibrium warming T_{eq} is approached much more slowly because h_2 is typically an order of magnitude larger than h_1.

We calibrate the EBM parameters iteratively in a manner similar to the tuning procedure outlined by *Geoffroy et al.* [2013b] (see supporting information for details). We fit the analytical solution for the upper layer temperature (6) to the area-averaged SST anomaly T_1 in each GCM, and we constrain equation (3) with the sea surface heat flux anomaly N_o. This allows us to calibrate our five free parameters. Convergence is achieved after a small number of iterations, and we are able to accurately reproduce the response of each GCM with the EBM (see Figure S2 in the supporting information and a summary of parameter values in Table S1).

Our estimate for the depth scale H across the calibrated two-layer EBMs is of the correct magnitude and correlates strongly ($R = 0.79$) with the depth of heat penetration $D_{80\%}$ as diagnosed within the CMIP5 models (Figure 5a). As could be anticipated from the close relationship between $D_{80\%}$ and the AMOC depth metric D_{AMOC} identified previously (Figure 3a), H is also strongly correlated ($R = 0.87$) with D_{AMOC} (Figure 5b). We previously pointed out (Figure 3b) a strong connection between D_{AMOC} and the AMOC stream function maximum, M_{AMOC}, which regulates the rate of heat transport from the mixed layer into the ocean interior. Likewise, the analogous parameter in the two-layer EBM, q, is found to be strongly correlated with both H ($R = 0.89$) and M_{AMOC} ($R = 0.84$); see Figures 5c and 5d and Table S2 in the supporting information. Our parameter correlations are not sensitive to the choice of $h_1 = 100$ m and are reproduced if we allow h_1 to vary across models. Remarkably, this simple two-layer ocean model, constrained only by SST and surface heat fluxes, captures essential features of the intermodel spread in ocean circulation and heat storage found within the ensemble of coupled GCMs.

In agreement with *Geoffroy et al.* [2013b], who perform a similar EBM calibration, we see that most of the spread in the equilibrium temperature T_{eq} comes from intermodel variability in the feedbacks λ_o, as opposed to $\mathcal{F}_o$ (Figure 5e). However, in contrast to our results, *Geoffroy et al.* [2013b] find a small negative correlation between H and q. We suggest that this is due to methodological differences. In particular, *Geoffroy et al.* [2013b] include the ocean mixed layer, the atmosphere, and the land domain in the upper layer of the EBM, while here we have focused on the ocean domain. We also note that we find a significant correlation ($R = 0.81$) between ε and q (Figure 5f), which may reflect the complex relationship between efficacy and the ocean circulation that sets the evolving pattern of surface heat uptake.

We take the remarkable consistencies between coupled GCMs and calibrated EBMs as evidence that the two-layer parameters can be understood in terms of ocean properties (i.e., strength and depth of the AMOC). This further implies that the two-layer calibration produces results that are physically meaningful. We can thus use the EBM to gain insight into the role of AMOC in transient climate change. For example, a deep and strong AMOC results in a deep penetration of the temperature signal. Within the two-layer EBM, this is represented by a thick layer h_2 and a high rate of heat exchange between the mixed layer and the deep ocean, setting a large effective ocean heat capacity and delaying the SST response to forcing. Such
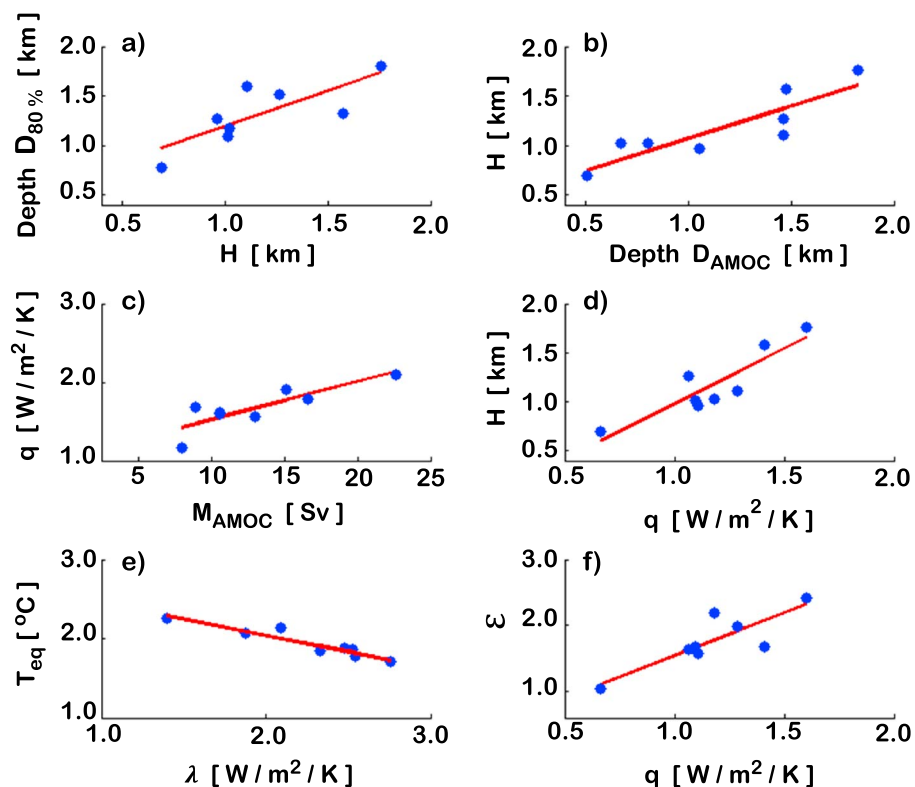
Figure 5. Correlations among GCM variables and calibrated EBM parameters with correlation coefficients R and p values p (a) $D_{80\%}$ and H, ($R = 0.79$, $p < 0.03$); (b) H and D_{AMOC} ($R = 0.87$, $p < 0.01$); (c) q and M_{AMOC} ($R = 0.84$, $p < 0.01$); (d) H and q ($R = 0.89$, $p < 0.01$); (e) T_{eq} and λ_o ($R = -0.94$, $p < 0.01$); and (f) ε and q ($R = 0.81$, $p < 0.01$).

is the case for NorESM1-M, which has the thickest h_2 and the largest q (Table S1) and exhibits very slow warming following CO_2 quadrupling (Figure 1a).

We can also apply the two-layer EBM to quantify the relative roles of ocean processes and climate feedbacks in setting the intermodel spread in climate response. We separate the parameters into two groups: those related to the ocean circulation (q, h_2, and ε) and those related only to the equilibrium warming (λ_o and $\mathcal{F}_o$). We point out that ε cannot be described simply as an ocean parameter because it depends on the interaction between regional ocean circulations and atmospheric feedbacks [*Armour et al.*, 2013; *Winton et al.*, 2010; *Rose et al.*, 2014]. However, q, h_2, and ε are strongly correlated with each other but not significantly correlated with λ_o and $\mathcal{F}_o$ (Table S2). Hence, in the context of intermodel spread, we treat ε as a parameter linked to the ocean circulation. We run the two-layer EBM once again, with $\mathcal{F}_o$ and λ_o specified to the values we diagnosed from each individual GCM calibration, but with q, h_2, and ε, fixed to ensemble-mean values (Figure 1c). Together, variations in λ_o and $\mathcal{F}_o$ appear to account for a substantial portion of the intermodel spread in SST response seen in Figure 1a, consistent with the findings of *Geoffroy et al.* [2012].

Nevertheless, variations in q, h_2, and ε must be taken into account to obtain the full spread of climate responses in CMIP5. The role of the ocean is particularly important within models that exhibit notably shallow or deep penetration of heat. For example, comparing Figures 1a and 1c, we see that the SST responses of CNRM-CM5 (weakest AMOC and shallowest heat storage) and NorESM1-M (strongest AMOC and deepest heat storage) are not well reproduced by the EBM under variations in feedbacks alone: SST is underestimated for CNRM-CM5 and overestimated for NorESM1-M. Running the two-layer EBM with GCM-specific q, h_2, and ε, but with ensemble-mean λ_o and $\mathcal{F}_o$, shows that ocean processes are indeed essential to understanding the behavior of individual models (Figure 1d) and that variations can yield an SST range of order $\sim 1°C$ after several decades. However, this spread is smaller than the spread due to feedbacks and forcing (Figure 1c) and also smaller than the intermodel differences in the CMIP5 responses (Figure 1a).

These results suggest that although feedbacks λ_o set much of the intermodel variability in the SST response, the ocean circulation plays an important role as well. That is, even if each GCM was governed by the same climate feedback, differences in ocean processes would still yield a notable range of SST responses. Within the two-layer EBM framework, these ocean differences can be understood in terms of an effective ocean heat capacity (set by h_2 and q) and an efficacy of heat uptake ε. Within the ensemble of GCMs, differences in the effective heat capacity can be understood in terms of variations in the depth of heat storage, which in turn reflects the depth and strength of the AMOC.

4. Discussion and Conclusions

We have identified an important role of the upper AMOC cell for regulating heat storage in the World Ocean as represented in an ensemble of state-of-the-art models. Our analysis of CMIP5 GCMs reveals that the AMOC is a major source of intermodel variability in the ocean's effective heat capacity and in the rate at which the heat anomaly is exported from the mixed layer downward (see *Medhaug and Furevik* [2011] for AMOC variability across CMIP3 models). Models with a deeper and stronger overturning circulation store more heat at intermediate depths, which delays the surface temperature response on multidecadal time scales.

We note the possibility that other vertical heat transport processes could be correlated with the strength and depth of the AMOC and thus would be neglected in our analysis. However, we have found that a substantial portion of the global ocean heat uptake occurs within a relatively small region in the North Atlantic and that anomalous heat is advected to depth along the upper AMOC cell. The AMOC can thus be expected to strongly influence the depth of global heat penetration. Several studies [e.g., *Xie and Vallis*, 2011; *Winton et al.*, 2013; *Rugenstein et al.*, 2013] have found that weakening of the AMOC can also substantially affect the depth of heat penetration through the redistribution of the background heat content. While changes in AMOC do occur within the CMIP5 GCMs under $4 \times CO_2$ forcing, we find no significant correlations between the magnitudes of the AMOC weakening or shoaling and the depth of heat storage across the ensemble (see supporting information). Thus, the diversity of AMOC strengths and depths across models appears to be the larger source of intermodel spread in the depth of heat penetration.

To quantify the relative influence of ocean processes versus climate feedbacks in setting the spread of CMIP5 temperature responses, we have employed a simple two-layer ocean model calibrated to each GCM. While much of the intermodel spread is attributed to feedback variations, ocean parameters are found to be important as well, and critical to the response of those models with very deep (or shallow) AMOC cells.

Our results have implications for understanding the climate response to greenhouse forcing and for improving the long-term prognostic power of models. Our findings suggest that a good representation of the AMOC is essential for accurately simulating ocean heat storage and transient warming. These conclusions point to the value of measuring and studying AMOC properties as the circulation evolves under global warming conditions.

References

Andrews, T., J. M. Gregory, M. J. Webb, and K. E. Taylor (2012), Forcing, feedbacks and climate sensitivity in CMIP5 coupled atmosphere-ocean climate models, *Geophys. Res. Lett.*, *39*, L09712, doi:10.1029/2012GL051607.

Armour, K. C., C. M. Bitz, and G. H. Roe (2013), Time-varying climate sensitivity from regional feedbacks, *J. Clim.*, *26*, 4518–4534, doi:10.1175/JCLI-D-12-00544.1.

Boé, J., A. Hall, and X. Qu (2009), Deep ocean heat uptake as a major source of spread in transient climate change simulations, *Geophys. Res. Lett.*, *36*, L22701, doi:10.1029/2009GL040845.

Geoffroy, O., D. Saint-Martin, and A. Ribes (2012), Quantifying the sources of spread in climate change experiments, *Geophys. Res. Lett.*, *39*, L24703, doi:10.1029/2012GL054172.

Geoffroy, O., D. Saint-Martin, D. J. L. Olivié, A. Voldoire, G. Bellon, and S. Tytéca (2013a), Transient climate response in a two-layer energy-balance model. Part I: Analytical solution and parameter calibration using CMIP5 GCM experiments, *J. Clim.*, *26*, 1841–1857, doi:10.1175/JCLI-D-12-00195.1.

Geoffroy, O., D. Saint-Martin, G. Bellon, A. Voldoire, D. J. L. Olivié, and S. Tytéca (2013b), Transient climate response in a two-layer energy-balance model. Part II: Representation of the efficacy of deep-ocean heat uptake and validation for CMIP5 GCMs, *J. Clim.*, *26*(6), 1859–1876, doi:10.1175/JCLI-D-12-00196.1.

Gregory, J., and M. Webb (2008), Tropospheric adjustment induces a cloud component in CO2 forcing, *J. Clim.*, *21*, 58–71, doi:10.1175/2007JCLI1834.1.

Gregory, J. M. (2000), Vertical heat transports in the ocean and their effect on time-dependent climate change, *Clim. Dyn.*, *16*(7), 501–515, doi:10.1007/s003820000059.

Hansen, J., G. Russell, A. Lacis, I. Fung, D Rind, and P. Stone (1985), Climate response times: Dependence on climate sensitivity and ocean mixing, *Science*, *229*, 857–859, doi:10.1126/science.229.4716.857.

Hansen, J., Mki. Sato, P. Kharecha, and K. von Schuckmann (2011), Earth's energy imbalance and implications, *Atmos. Chem. Phys.*, *11*, 13,421–13,449, doi:10.5194/acp-11-13421-2011.

Held, I. M., M. Winton, K. Takahashi, T. Delworth, F. Zeng, and G. K. Vallis (2010), Probing the fast and slow components of global warming by returning abruptly to preindustrial forcing, *J. Clim.*, *23*, 2418–2427, doi:10.1175/2009JCLI3466.1.

Hoffert, M. I., A. J. Callegary, and C.-T. Hsieh (1980), The role of deep sea heat storage in the secular response to climatic forcing, *J. Geophys. Res.*, *85*(C11), 6667–6679, doi:10.1029/JC085iC11p06667.

Kuhlbrodt, T., and J. M. Gregory (2012), Ocean heat uptake and its consequences for the magnitude of sea level rise and climate change, *Geophys. Res. Lett.*, *39*, L18608, doi:10.1029/2012GL052952.

Li, C., J.-S. von Storch, and J. Marotzke (2012), Deep-ocean heat uptake and equilibrium climate response, *Clim. Dynam.*, *40*, 1071–1086, doi:10.1007/s00382-012-1350-z.

Medhaug, I., and T. Furevik (2011), North Atlantic 20th century multidecadal variability in coupled climate models: Sea surface temperature and ocean overturning circulation, *Ocean Sci.*, *7*, 389–401, doi:10.5194/os-7-389-2011.

Raper, S. C. B., and U. Cubasch (1996), Emulation of the results from a coupled general circulation model using a simple climate model, *Geophys. Res. Lett.*, *23*, 1107–1110, doi:10.1029/96GL01065.

Raper, S., J. Gregory, and R. Stouffer (2002), The role of climate sensitivity and ocean heat uptake on GCM transient temperature response, *J. Clim.*, *15*, 124–130.

Rose, B. E. J., K. C. Armour, D. S. Battisti, N. Feldl, and D. D. B Koll (2014), The dependence of transient climate sensitivity and radiative feedbacks on the spatial pattern of ocean heat uptake, *Geophys. Res. Lett.*, *41*, doi:10.1002/2013GL058955.

Rugenstein, M. A. A., M. Winton, R. J. Stouffer, S. M. Griffies, and R. Hallberg (2013), Northern high-latitude heat budget decomposition and transient warming, *J. Clim.*, *26*, 609–621, doi:10.1175/JCLI-D-11-00695.1.

Stouffer, R. J. (2004), Time scales of climate response, *J. Clim.*, *17*, 209–217, doi:10.1175/1520-0442(2004)017<0209:TSOCR>2.0.CO;2.

Taylor, K. E., R. J. Stouffer, and G. A. Meehl (2012), An oveview of CMIP5 and the experiment design, *Bull. Am. Meteorol. Soc.*, *93*, 485–498, doi:10.1175/BAMS-D-11-00094.1.

Wigley, T. M. L., and S. C. B. Raper (1987), Thermal expansion of sea water associated with global warming, *Nature*, *330*, 127–131, doi:10.1038/330127a0.

Winton, M., K. Takahashi, and I. M. Held (2010), Importance of ocean heat uptake efficacy to transient climate change, *J. Clim.*, *23*, 2333–2344, doi:10.1175/2009JCLI3139.1.

Winton, M., S. M. Griffies, B. L. Samuels, J. L. Sarmiento, and T. L. Frölicher (2013), Connecting changing ocean circulation with changing climate, *J. Clim.*, *26*, 2268–2278, doi:10.1175/JCLI-D-12-00296.1.

Xie, P., and G. K. Vallis (2011), The passive and active nature of ocean heat uptake in idealized climate change experiments, *Clim. Dyn.*, *38*, 667–684, doi:10.1007/s00382-011-1063-8.